MODERNISING, UPGRADING AND RECOMMISSIONING THE INDOOR ANTENNA RANGE AT STELLENBOSCH UNIVERSITY

D. M. P. Smith*, D. B. Davidson*, A. Bester* and J. Andriambeloson*

* *Department of Electrical and Electronic Engineering, Stellenbosch University, Stellenbosch 7600, South Africa. Email: davidson@sun.ac.za*

Abstract: This paper describes the upgrade to the indoor antenna range at Stellenbosch University. The previous measurement process relied upon obsolescent control equipment and undocumented software; it was critical that these be replaced. Now, the antenna range supports three measurement types using a commercial integrated measurement control system that provides support for high gain and low gain antennas over a wide frequency range. These are spherical near-field, planar near-field and conventional far-field measurements, with the potential to implement cylindrical near-field. The antenna range potentially supports operations from 1 GHz up to 26.5 GHz, though the currently available probes do not cover the full band. The main physical upgrade was performed during October 2014, though investigations had already begun in 2011, and some supplementary tasks were still ongoing at the time of writing. Several innovative commissioning tests have been undertaken, some of which are only possible with near-field metrology, and these are described in the paper.

Key words: Indoor Antenna Range, Spherical Near-Field Measurements, Planar Near-Field Measurements, Far-Field Measurements

1. INTRODUCTION

Stellenbosch University's antenna range was originally built over twenty five years ago under the direction of Prof J. H. Cloete, with the majority of components designed and manufactured internally by members of staff [1]. At around much the same time, a number of other antenna ranges were built in South Africa, including the indoor range at the Pretoria campus of the Council for Scientific and Industrial Research [2], the compact range at Pretoria University [3], and the outdoor range at Paardefontein [4].

This reflected major interest in antenna engineering at the time, which was driven largely, although not exclusively, by defence applications. All of these antenna ranges have provided excellent service over many years to the antenna engineering community in South Africa. Also, they have proven very attractive to overseas companies, particularly the outdoor range at Paardefontein. Recently, the national focus on the Square Kilometre Array radio telescope has given renewed impetus to antenna engineering [5].

Stellenbosch University's facility originally comprised a polarisation axis rotator mounted on an automated planar scanner and cylindrical axis rotator mounted on a manual translation track that permitted these measurement types: cylindrical near-field (CNF), planar near-field (PNF), and far-field (FF) cuts. While this facility was still functional, major components were no longer supported nor properly understood, hindering continual support of this facility. Firstly, the facility relied upon a venerable HP 8510 vector network analyser (VNA), which has not been supported by the manufacturer for several years (originally Hewlett Packard, then Agilent, presently Keysight Technologies). Also, the control equipment relied upon obsolete software, that was effectively undocumented, and legacy drivers. Finally, a number of crucial components were no longer supported, such as the controller for the stepper motors.

With commercial simulation software readily available, it is now the ability to make high quality measurements that differentiates leading research institutes in the field. Access to these facilities is limited, due to the expense of RF measurement equipment, and specialist operators are required to obtain the best results. During the lifespan of this facility to date, well over two hundred post graduate students have been able to receive training at the facility, providing a number of them with a crucial component in their research. This facility is also used in the final year course on high frequency systems. These considerations made modernising and upgrading the facility a priority.

Near-field (NF) metrology has several advantages over FF metrology, with the most obvious being that the probe is not constrained to being in the FF of the antenna under test (AUT). When the facility was originally commissioned, NF metrology was in its infancy [6, 7], and facilities were custom-made, both in terms of hardware and software. In the interim, commercial products, with ongoing technical support, have become available [8]. As our antenna range is a general purpose facility, it was upgraded as a NF range, given the flexibility offered by such a system, although some initial consideration was given to converting the anechoic chamber into a tapered range, similar to [9].

In this paper, the upgrade of this facility is detailed. This begins with an overview of the upgrade process, specifically the changes made to support the new components. This is followed by a description of the functions of the components, focusing on the options provided by the NF measurement types. Thereafter, a description of the measurement setup is provided, including the calibration process required prior to performing a measurement. The paper concludes

with initial results using the facility; several innovative commissioning tests, which represent new contributions in the context of this range; and an outline of ongoing and planned work to further improve the facility.

2. UPGRADE PROCESS

While the manufacture of antenna measurement systems is a specialised field in general, this is particularly true for NF ranges. Therefore, Nearfield Systems, Inc. (NSI), a US based company, was contracted to drive the upgrade of Stellenbosch University's facility [10]. This company has been providing hardware, software and customer support for antenna metrology for over a quarter of a century. Of particular interest is the integration of NSI's components with that of Keysight Technologies' range of VNAs, as our research group had extensive experience using their VNAs.

Both planar motions and spherical motions are required to provide support for both high gain and low gain antennas, as each motion type is appropriate for a different gain type, with this upgrade including both in an integrated system. The 700S-30 was identified as an appropriate model for the spherical motions, in supporting antennas up to 0.5 m in diameter and up to 18 kg in mass. This spherical near-field (SNF) scanner supports medium and low gain antennas in sampling the full sphere around the AUT and the existing PNF scanner supports high gain antennas in sampling a finite sector of the forward hemisphere of the AUT.

Before the upgrade was initiated, the state of components was catalogued, to determine which components to replace and which to retain. The absorber material, PNF scanner and Z Track were in good condition, despite providing over a quarter century of service. For reasons outlined above, it is useful to have *both* PNF and SNF scanners available, and it proved cost effective to integrate these into one system, making use of the Z Track to shift the SNF scanner to allow for both measurement types – and potentially CNF – using the same equipment. It should be noted that this facility can only support one measurement type at any given time.

Although still functional, the cylindrical axis rotator was rendered redundant by the procurement of the SNF scanner. Similarly, the new control equipment rendered the motors and the encoders of the PNF scanner redundant. While the SNF scanner is designed to be mounted on the floor, a wheeled base was designed at Stellenbosch University to manually shift it along the Z Track to the desired separation from the probe. This base positions the AUT at the anechoic chamber's mean height, maximising the scan area and positioning the AUT in the quiet zone.

3. SYSTEM COMPONENTS

Stellenbosch University's antenna range comprises the control equipment, primarily housed in the control room; the motion stages, housed in the anechoic chamber; and the control and RF cabling connecting the various components in and between these two rooms. The control equipment comprises the motion stage controllers; the workstation running the data processing software; and the VNA, which acts as both the RF source and receiver. The motion stages comprises the various motors, motor drivers and support structures for the planar and spherical scanners. All these components, and the probes, are described in this section.

3.1 Control Room

The control room forms part of a larger workspace, which includes the laboratory manager's office and the storage area for the antenna range's interchangeable components. This room shares a dry wall with the anechoic chamber, which contains the interface for the control and RF cabling to pass between these two rooms and the door for personnel to gain access to the anechoic chamber. The control room has a grounded workbench, on which the majority of the control and measurement equipment are housed.

The user utilises a desktop workstation in order to perform measurements. The data processing software is installed on this workstation, which allows the user to interact virtually with the hardware, with the complicated process of controlling and synchronising the motor movements with the measurement sampling hidden from the user. However, the user must understand the limits of the antenna range, as it is possible to override the hardware and software safeguards during the calibration process.

In taking the measurements, the VNA is a core component. The PNA-X 5242A was identified as an appropriate model due to its performance, integration with NSI components, and our familiarity with its predecessors. It is also used for numerous other measurement types [11]. While the new VNA covers the same frequency range as the previous one, the speed at which it switches between frequencies is much faster. This allows the two scanners to move continually during measurements, greatly speeding up the process.

The control and synchronisation of the motor movements with the measurement sampling is performed by the primary controller. This device converts requests made by the user in the data processing software into commands for both the VNA and the motors. It also records the motor movements and the measured samples. These records are synchronised and stored on the desktop workstation. Once the measurement set has completed, the user interacts with the data processing software to generate the desired results.

Additionally, the primary controller directly controls the SNF scanner's motors and indirectly controls the PNF scanner's motors through the secondary controller. Whilst part of the control equipment, the secondary controller is housed inside the anechoic chamber behind the X Track to reduce the length of, and therefore loss in, the power cabling. Due to the mass of the Y Tower, motor drivers are utilised to provide the x stage and y stage with sufficient power. None of the other stages require motor drivers.

The control room is equipped with an uninterruptible power supply in the event of a power outage, allowing the components to be shut down gracefully. No mechanical

damage is expected, as the lead screws of the PNF scanner hold the Y Tower and the probe in place. A minimum measurement set is lost, as the data is stored on the desktop workstation after each scan. However, the motor positions require recalibration after a power outage, with the option of resampling a portion of the scan area for verification.

3.2 Anechoic Chamber

The anechoic chamber is a rectangular room of dimension 9.1 m (L) × 5.5 m (W) × 3.6 m (H). Several modifications were required when the chamber was constructed in the 1980s, as this room was originally an acoustic chamber. To shield the room from external signals, the interior surfaces were covered with aluminium sheeting, with the joints soldered together to create a Faraday cage. As is usual with an anechoic chamber, the interior surfaces of the flooring, walls and ceiling were covered with absorber pyramids.

The back wall is covered with commercially supplied absorber pyramids of 18 inch (450 mm) in height, with the other surfaces covered with absorber pyramids of 12 inch (300 mm) in height. The absorption of these pyramids at a particular frequency is better the taller the pyramid, with 18 inch pyramids specified down to 500 MHz and 12 inch pyramids down to 1 GHz. There is a walkway made from absorber material running parallel to the Z Track, allowing personnel to traverse the length of the anechoic chamber.

Although the walkway is made out of absorber material, it has different properties to the pyramids. Using the ability of the SNF scanner to rotate both rotation axes beyond 360°, it is possible to perform SNF measurements over a complete sphere with or without orientating the AUT in the direction of the walkway. This will be used later in this paper to quantify the performance variance between the pyramids and the walkway.

To screen the AUT from the reflective surfaces of the PNF scanner, two wooden panels are mounted onto the Y Tower, with the surface of these panels facing the AUT covered with absorber pyramids. Similarly, to screen the probe from the reflective surfaces of the SNF scanner, the L Bracket is covered with absorber pyramids. In both cases, these absorber pyramids are 8 inch (200 mm) in height, and are specified down to 1 GHz. However, the reflective surfaces of the SNF base remain untreated.

The sections of the floor and roof that the Y Tower passes along during PNF measurements are free of absorber pyramids, to avoid fouling the Y Tower. The lead screw for the X Track runs above the floor level, making it difficult to screen this section of the floor with absorber pyramids. As there is no hardware at ceiling level, the aluminium sheeting here was covered with non-reflective material. Over this, velcro strips were installed, so that absorber pyramids could be attached during SNF measurements.

A section of the floor behind the X Track has been cleared of absorber material to house the secondary controller. The opening is larger than the volume of this controller to allow the control cabling to be connected to the back panel and to give personnel access to the switches on the front panel. Additionally, space was made to not block its cooling vent on the side panel. While non-ideal from a RF interference point of view, this controller is housed near the PNF scanner to provide its motors with sufficient power.

3.3 Planar Scanner

The PNF scanner comprises the X Track embedded in the floor of the anechoic chamber, the Y Tower mounted on the X Track, and the polarisation stage mounted on the Y Tower. To move the probe along the x axis, the *x* stage translates the Y Tower along the X Track. To move the probe along the y axis, the *y* stage translates the pol stage along the Y Tower. To rotate the probe around the polarisation axis, the pol stage rotates the probe. These three stages are controlled by the secondary controller.

The existing X Track and Y Tower were retained, with the two motion stages replaced and the pol stage redesigned. The *x* and *y* stages comprise motors and drivers that move the probe over a 2.6 m (x axis) × 2.0 m (y axis) scan area, with minimum step sizes of 0.025 mm (x axis) and 0.0125 mm (y axis) at speeds of 0.1 m/s (x axis) and 0.05 m/s (y axis). The pol stage comprises a motor and rotary joint, that rotates the probe between polarisations, with a minimum step size of 0.0125° at a speed of 20°/s.

The gap between the absorber panels on the Y Tower can be adjusted to accommodate probes of varying dimension. However, the wider the gap, the greater the surface area of the reflective surfaces of the Y Tower that is seen by the AUT. Therefore, to maximise the probe support and to maximise the Y Tower absorber coverage, the pol stage is housed behind the absorber panels, with only cabling and a support beam passing between the absorber panels. This does limit the probe mass supported by the Y Tower.

There are three different safety mechanisms in place to prevent the *x* stage and the *y* stage from derailing the PNF scanner. Soft limits restrict the movements of the PNF scanner to within the bounds set by limit switches mounted on the X Track and the Y Tower. Hard limits cut the power to the motors in the event that these switches are passed, with hard stops mounted on the ends of the X Track and the Y Tower. The pol stage is fitted with a rotary joint to prevent the cabling from wrapping around the Y Tower.

The PNF and SNF scanners are depicted in Figure 1.

3.4 Spherical Scanner

The SNF scanner comprises the 700S-30 scanner mounted on the SNF scanner base, which is mounted on the Z Track, which is embedded in the floor of the anechoic chamber. To move the AUT along the z axis, the SNF scanner is manually translated along the Z Track. To rotate the AUT around the θ axis, the θ stage rotates only the L Bracket of the SNF scanner. To rotate the AUT around the ϕ axis, the

Figure 1: Anechoic Chamber

Figure 2: Spherical Near-Field Scanner

ϕ stage rotates the AUT. As the Z Track is not absolutely flat, the SNF scanner is levelled after each translation.

The existing Z Track was retained, with the SNF base manufactured internally at our university, with the other components forming part of the upgrade. The θ stage and the ϕ stage comprise motors and rotary joints that rotate the AUT over a 360° (θ axis) $\times$ 360° (ϕ axis) spherical scan area, with step sizes of 0.0125° (both) at speeds of 20°/s (ϕ axis) and 7.3°/s (θ axis). There are three measurement setups: 180° (θ axis) $\times$ 360° (ϕ axis), 360° (θ axis) $\times$ 180° (ϕ axis) and the redundant 360° (θ axis) $\times$ 360° (ϕ axis).

The AUT is offset from the mounting interface of the SNF scanner. This is done to reduce SNF measurement times by reducing the offset between the AUT and the θ axis, with this axis running through the centre of the SNF base. Also, this protects the absorber pyramids by offsetting the volume in which the AUT and RF cabling rotate during SNF measurements from the volume occupied by the absorber pyramids on the SNF scanner. However, this does limit the AUT mass supported by the SNF scanner.

Unlike for the PNF scanner, no rotation of the ϕ stage nor the θ stage could potentially derail the SNF scanner. Soft limits on the θ stage are used to align the AUT as part of the calibration process and to prevent the cabling from wrapping around the SNF scanner. The θ stage has no hard limits, as the 360° rotations that form part of SNF measurements prohibit their use. The ϕ stage has no limits, with alignment determined with a level and a rotary joint preventing the cabling from wrapping around the scanner.

The SNF scanner is depicted in Figure 2.

3.5 Probes

The operational properties of the four currently available probes are listed in Table 1. While the rectangular probes are suitable for both measurement types, the horn probe (RGP-10) is restricted to SNF measurements, due to the nulls in the forward hemisphere of the radiation pattern of this probe, which would cause errors in the PNF probe correction algorithm. If required, users can provide their own probes, with compatible mounting brackets, and implement their own probe correction on the NF data.

Table 1: Probe Operational Properties

Probe	Frequency Range	Measurement Type
RGP-10	0.7–5.0 GHz	SNF
WR137	5.85–8.2 GHz	PNF, SNF
WR90	8.2–12.4 GHz	PNF, SNF
WR62	12.4–18 GHz	PNF, SNF

As the antenna range supports PNF and SNF measurements, with the potential to include CNF measurements, it is desirable to have probes suitable for both measurement types over as wide a frequency range as possible. However, the size and weight of low frequency rectangular probes would strain the load capacity of the scanners. Therefore, a horn probe is used, which is smaller and lighter than the comparable rectangular probes and which has a wider operational band than the comparable rectangular probes.

Each probe has a kit comprising absorber collar, mounting bracket and waveguide to coaxial transition, as depicted in Figure 3. The absorber collar hides the reflective surfaces of the RF cabling and mounting interface from the AUT. The mounting bracket allows the probes to be mounted on both scanners. For the rectangular probes, the waveguide to coaxial transition is positioned behind the absorber collar, while for the horn probe it is in front of the absorber collar, but hidden from the AUT by the horn's flanges.

3.6 Anechoic Chamber Layout

The anechoic chamber layout is depicted in Figure 4. The PNF scanner is the Y Tower mounted on the X Track and

(a) Horn Probe (b) Rectangular Probe

Figure 3: Probe Kits

the SNF scanner is the L Bracket mounted on the Z Track. The probe mounting interface is in front of the absorber panels, limiting the maximum AUT to probe separation to 6.0 m, and the AUT mounting interface is on the L Bracket. The Z Track is offset from the mean width to accommodate the walkway. While the Y Tower can transverse the full X Track, its nominal position is aligned with the Z Track. If the dimensions or mass of the AUT exceed the limits of the SNF scanner, the SNF scanner could be moved out of the way, with a suitable stand manufactured for the AUT. Only PNF measurements could be made in this case.

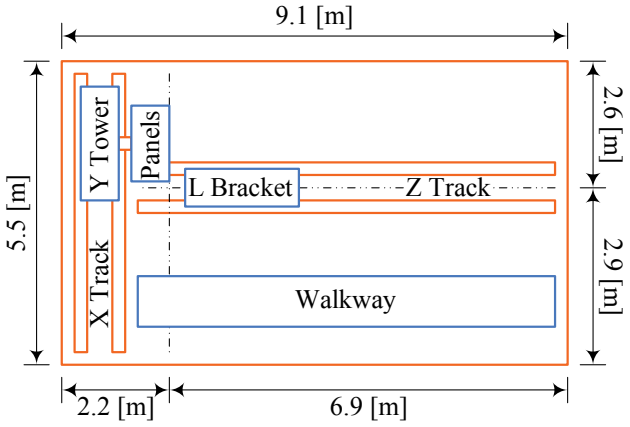

Figure 4: Anechoic Chamber Layout

The coordinate system of the anechoic chamber is depicted in Figure 5. Positive θ rotation is clockwise as seen from above the AUT and positive ϕ rotation is counter clockwise as seen from behind the AUT. As seen from in front of the probe, positive x translation is leftward, positive y translation is upward, positive z translation is backward and positive polarisation rotation is clockwise. During calibration, the x stage, y stage and θ stage move in their negative directions to determine their nominal positions. The definition of θ and ϕ rotations are opposite to those normally used; for our facility, the AUT moves during SNF measurements, whilst the probe remains stationary. (Conventionally in antenna theory, the AUT is stationary, at the centre of the coordinate system, and the fields around it are probed as a function of θ and ϕ.)

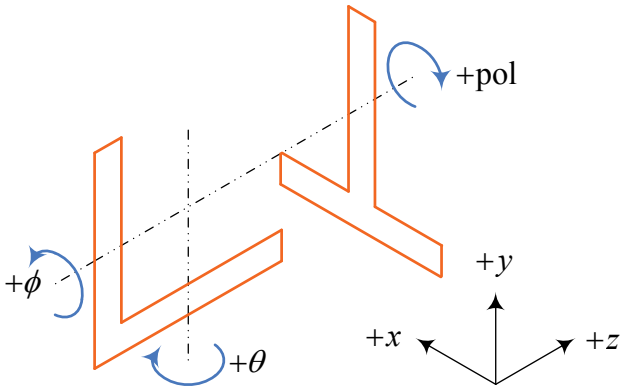

Figure 5: Anechoic Chamber Coordinate System

3.7 *Antenna Range Layout*

The control interface is depicted in Figure 6. The primary controller converts the user's interactions with the desktop workstation into synchronised movements of the SNF scanner (directly) and PNF scanner (via the secondary controller) with measurement sampling by the VNA. The x stage and y stage require drivers to move the Y Tower.

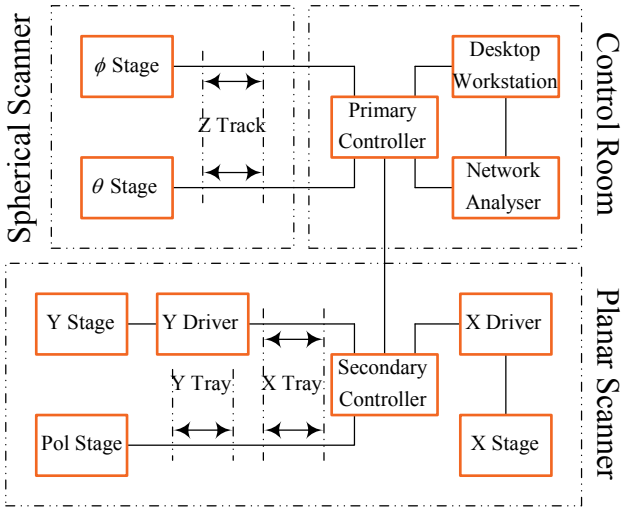

Figure 6: Control Interface

The RF interface is depicted in Figure 7. The VNA compares the signal transmitted by the AUT with the signal detected by the probe and amplified by the amplifier. The θ stage, ϕ stage and pol stage are fitted with rotary joints.

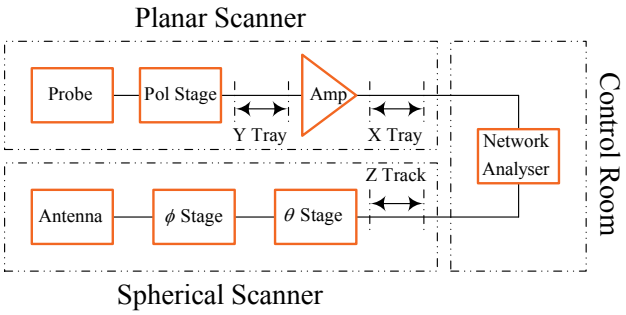

Figure 7: RF Interface

The power interface is depicted in Figure 8. The secondary controller and drivers are housed in the anechoic chamber to provide the PNF scanner with sufficient power.

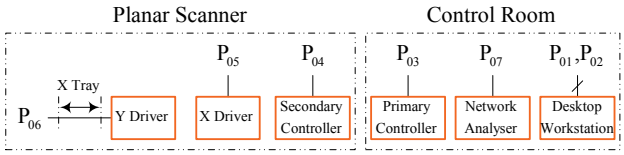

Figure 8: Power Interface

4. MEASUREMENT PROCESS

Making high quality measurements at an antenna range requires attention to NF and FF metrology theory in terms of understanding the motions of the scanners, setting up the measurement, designing a suitable mounting interface for the AUT, calibrating the antenna range and correcting for probe effects. All of these are described in detail in this section. While the mathematics surrounding NF to FF transformations are beyond the scope of this paper, a brief introduction into the theoretical background is given.

As FF patterns are the end result of most measurements, it would appear logical to place the probe in the FF — and indeed, this is a standard requirement in a far-field range. Generally, the FF is established at $2D^2/\lambda$ from the antenna, where D is the largest dimension of the antenna and λ is the wavelength [12]. This distance might be inadequate for high-precision measurements and could become excessive for electrically large antennas or low frequency measurements. In such cases, the probe is placed in the radiating NF, with NF to FF transformation used to compute the FF data [8].

During PNF measurements, the position and orientation of the AUT remains constant throughout, while the probe is twice moved over a planar surface in front of the AUT, with the orientation of the probe rotated 90° between scans to measure orthogonal polarisations. As only the forward hemisphere of the AUT is sampled, PNF measurements are best suited for high gain antennas. As the AUT remains at rest throughout the measurement, PNF measurements are best suited for antennas that are large, heavy and/or flimsy.

By contrast, during SNF measurements, the AUT is twice moved over a spherical surface in front of the probe, while the position and orientation of the probe remains constant for each scan, with the orientation of the probe rotated by 90° between scans for polarisation purposes. As the sphere around the AUT is sampled during SNF measurements, these measurements are best suited for low gain antennas. As the AUT is in motion throughout, SNF measurements are best suited for small, lightweight and sturdy antennas.

During PNF measurements, the orientation between the AUT and the probe varies throughout, with the probe sampling the AUT fields at angles off the probe's boresight. As such, the probe's radiation pattern should have no nulls in its forward hemisphere. While the main beam of a horn probe would be too narrow, a rectangular probe would have the desired radiation pattern. However, the operational band of a rectangular probe is limited, requiring multiple probes to span the full band at our facility.

By contrast, during SNF measurements, the orientation of the probe remains fixed on the AUT throughout, with the probe sampling the AUT fields on the probe's boresight. This allows a probe with a narrower main beam to be used, as the sector of the probe's radiation pattern that must be null-free is reduced. While rectangular and horn probes can be used, horn probes have the advantages of operating over a wider frequency range than rectangular probes and are lighter than rectangular probes at low frequencies.

4.1 Planar Near-Field Measurements

The probe motion during PNF measurements is depicted in Figure 9. The probe is translated the full y axis in one direction, then translated the sampling distance, Δx, in the x axis, before being translated the full y axis in the opposite direction. Once the full x axis is traversed, the probe is rotated and then it traces its path in the reverse direction. While both x over y and y over x are possible, y over x is the default as y translation is faster than x translation.

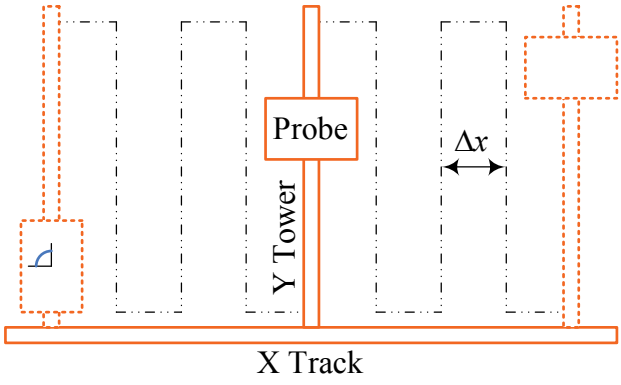

Figure 9: Planar Near-Field Measurement Motions

The PNF measurement setup is depicted in Figure 10. The probe travel length, L, is determined by the relationship

$$L \approx D + 2Z\tan\alpha \qquad (1)$$

where D is the AUT diameter, Z is the AUT-to-probe separation, and α is the scan angle. As the probe must be in the radiating NF, Z is usually set to 3λ. Since the probe must detect as much of the energy in the NF as possible, α is chosen large enough to encompass all the significant NF energy; typically, 40 dB below peak is used as the criterion.

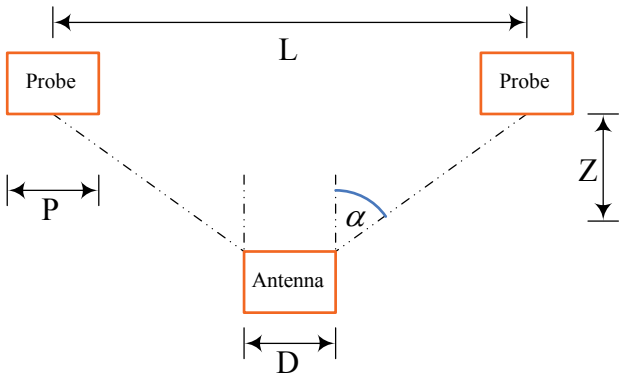

Figure 10: Planar Near-Field Measurement Setup

The SNF scanner can be shifted nearer the PNF scanner and/or a bracket can be mounted on the SNF scanner's mounting interface to reduce the AUT to probe separation. This would reduce the probe travel length for a given scan angle, reducing the measurement time. However, the probe must remain in the radiating NF. Similarly, the bracket cannot overload the SNF scanner's bending moment nor misalign the AUT from the centre of rotation of the ϕ stage.

4.2 *Spherical Near-Field Measurements*

The probe and AUT motions during SNF measurements are depicted in Figure 11. The AUT is rotated the full θ axis in one orientation, then rotated the sampling distance in the ϕ axis, before being rotated the full θ axis in the opposite direction. Once the full ϕ axis is rotated, the probe is rotated, before the AUT traces its path in the reverse direction. While both θ over ϕ and ϕ over θ are possible, ϕ over θ is the default as ϕ rotation is faster than θ rotation.

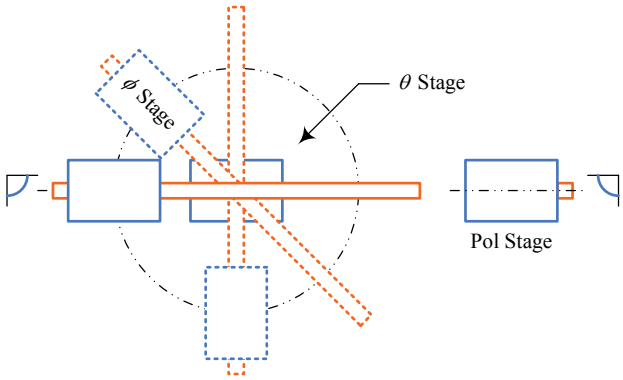

Figure 11: Spherical Near-Field Measurements Motions

The SNF measurement setup is depicted in Figure 12. The scan centre is the intersection of the θ and ϕ axes, with the probe aligned with the ϕ axis. MRS is the minimal radius sphere, which is the spherical volume around the scan centre that the AUT fills during SNF measurements. PSR is the probe scan radius, which is the distance between the probe and the scan centre. The smaller the minimal radius sphere, the shorter the measurement time. The shorter the probe scan radius, the lower the free space losses.

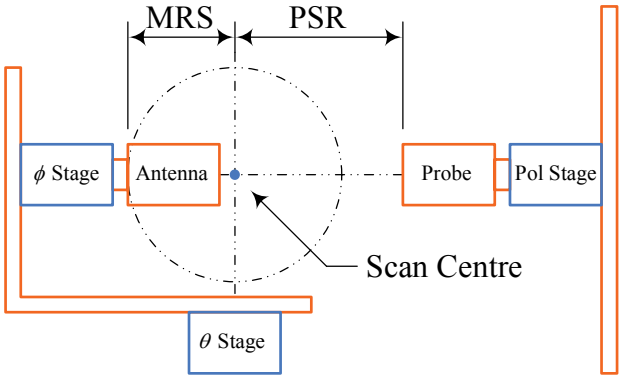

Figure 12: Spherical Near-Field Measurement Setup

A bracket can be mounted on the SNF scanner's mounting interface to place the AUT closer to the θ stage's centre of rotation. This would reduce the volume that the AUT fills, reducing the measurement time. However, this bracket must not overload the SNF scanner's bending moment nor misalign the AUT from the ϕ stage's centre of rotation. The SNF scanner can be shifted nearer the PNF scanner. However, the probe must remain in the radiating NF.

4.3 *Calibration Process*

Before the calibration process begins, the components in the antenna range are switched on, with the order equal to the inverse of the hierarchy of the control equipment: motor drivers; secondary controller; VNA; desktop workstation; primary controller; and data processing software. It is advisable to switch the VNA, the power amplifier and the cooling system on an hour before the measurement sampling starts to allow the temperature in the anechoic chamber and these components to stabilise.

Preceding calibration, it must be determined whether the AUT can indeed be measured at the range. This requires that the AUT operates at a frequency range compatible with the probes, that the AUT has an interface that is compatible with the SNF scanner, and that the AUT does not overload the SNF scanner's bending moment. While the choice between SNF and PNF measurements is usually determined by the antenna's directivity, the former might be excluded if the AUT is too heavy or fragile to be rotated.

Given this, the first step in the calibration process is to mount the AUT and the probe onto the scanners. This is required to determine the positioning of the SNF scanner

along the Z Track, as well as any resizing of the standoffs of the AUT's mounting bracket. To minimise measurement time, it is preferable to position the AUT as close as possible to the probe during PNF measurements, while it is preferable to position the AUT as close as possible to the centre of rotation of the θ stage during SNF measurements.

A mounting bracket was designed for the AUT, as depicted in Figure 13. The back interface is compatible with the mounting interfaces of the PNF and SNF scanners. While the front interface has several mounting holes, users can interchange it for one that is compatible with their AUT. The absorber collar, comprising 6 inch absorber pyramids, hides the reflective surfaces around the ϕ stage from the probe, with the components in front of the collar made of perspex. The gap in the collar is to allow cabling through.

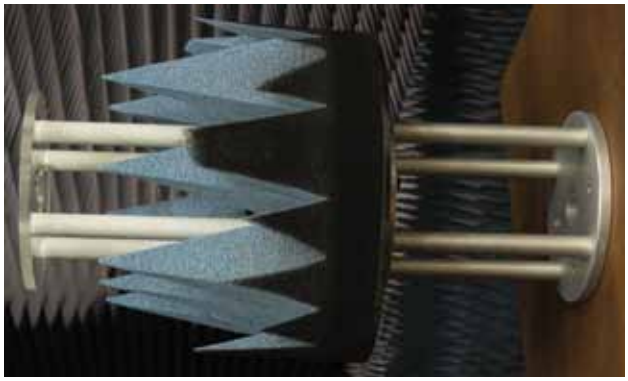

Figure 13: AUT Bracket

If the Z Track has been repositioned, the SNF scanner needs to be realigned, due to the non-ideal alignment of the Z Track with the floor of the anechoic chamber. When repositioning the Z Track, one should ensure that the RF cabling connected to the SNF scanner is the optimal length to minimise RF cable losses. Once the probe and the AUT have been mounted, they are aligned with each other for polarisation purposes. However, the data processing software can correct for misalignment during processing.

The polarisation setup for devices, both probes and AUTs, is depicted in Figure 14. The principal polarisation is at 0°, and this is when the connector is on the left of the device. The cross polarisation is at 90°, and this is when the connector is on top of the device. The definition for polarisation is when the user is in front of the device and looking at the device. Polarisation alignment is achieved by placing a spirit level on top of the probe for the pol stage and similarly on top of the AUT for the ϕ stage.

As no method to determine the positions of the x stage, y stage and θ stage has been implemented, their positions are calibrated each time their motors are switched on. Their motors are indexed by moving them in the direction of their safeguards, which are located at exact positions. Once these safeguards have been reached, the motors are able to reposition themselves relative to these positions. However,

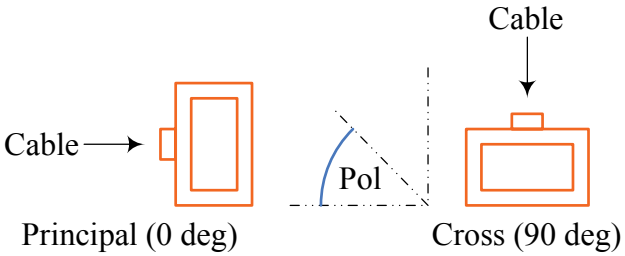

Figure 14: Polarisation Setup

a method to independently monitor whether the motors are moving as expected has not been implemented.

Once the calibration process has been completed, it is advisable to perform a few sanity checks. The power levels detected by the probe should drop when the probe's polarisation is rotated. For PNF measurements, one should ensure that the PNF scanner's motions will not crash the probe into the walkway. For SNF measurements, one should ensure that the cabling will not wrap around the SNF scanner. With the data processing software set on stability check, one should ensure that the RF cabling has been properly torqued.

Probe correction requires data about the probe in one of three forms: analytical model, simulation model or measurement data. Analytical models are suitable for probes with predictable radiation patterns and that have low on-axis cross polarisation levels, such as rectangular probes [13]. For complex probe types, such as horn probes, where the radiation pattern cannot be accurately predicted, simulated or measured data is required, with measurement data preferred due to manufacturing tolerances [14].

In the antenna range, probe correction forms part of the NF to FF transformation algorithm, with the option of selecting between an analytical model, only available for the three rectangular probes, or importing third party data, with measurement data available for the horn probe. With this option, users are free to import third party data for the rectangular probes or for their own probe, if needed. Otherwise, the raw NF data can be exported, allowing users to apply their own NF to FF transformations.

5. COMMISSIONING TESTS AND RESULTS

The commissioning of this facility is an ongoing process, as different measurements uncover new aspects of the facility. In this section, initial test of the facility and initial measurements using the facility are presented.

5.1 Stability Check

The stability check option has uncovered a stability problem with the RF cabling at the rear of the PNF scanner. With the system at rest, the RF cabling in the region of the amplifier is wiggled by hand, with the resulting phase change depicted in Figure 15. The phase does not return to the original value after the wriggle and the

magnitude of change that the phase undergoes during the wriggle is excessive. Therefore, replacement cables are being investigated. The SNF scanner has no such similar problem.

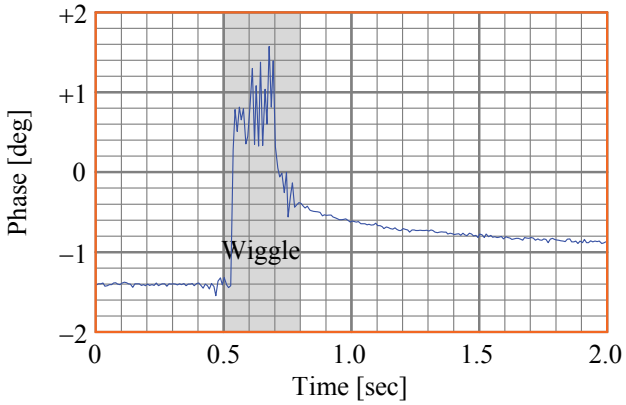

Figure 15: Stability Check

Before each measurement, a sample is taken at a point in the high energy zone of the AUT, and after each measurement, another sample is taken at the same point. The difference between these two measurements is an indication of the amplitude and phase drift during the measurement. Irrespective of frequency, our system has a ± 0.1 dB and $\pm 1^\circ$ drift for an hour long measurement. As an example, the stability check option is used to show that the rotation of the pol stage from 0° to 90° and back to 0° has a minimal effect on the amplitude and a marginal effect of the phase of the measurement, as depicted in Figure 16.

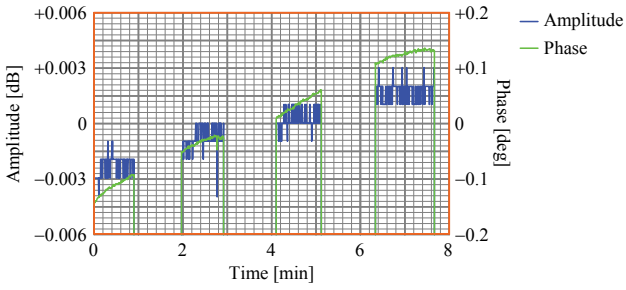

Figure 16: Drift Check

5.2 *Alignment Check*

As part of the installation process, a five point laser was used to align the axes of the five automated stages and to align the mounting interfaces of the pol and ϕ stages. During the calibration process, the distances from this alignment point to the negative limit switches along the X Track, along the Y Tower and in the θ rotation stage are used to realign the x, y and θ stages, while the pol and ϕ stages are aligned using a spirit level. While this mechanical alignment is accurate, machining tolerances for the mounting brackets could introduce deviations.

During initial testing, deviations of the order of ± 1 cm (x and y axes), $\pm 1^\circ$ (θ axis) and ± 1 mm (pol and ϕ mounting interface) have been recorded. These deviations have a greater effect at higher frequencies and on the phase, potentially leading to artefacts in the transformed FF patterns. As an example, two SNF measurements are taken, with a deliberate misalignment of the y axis introduced before the second measurement, resulting in the sharp contrast between the FF transformations depicted in Figure 17.

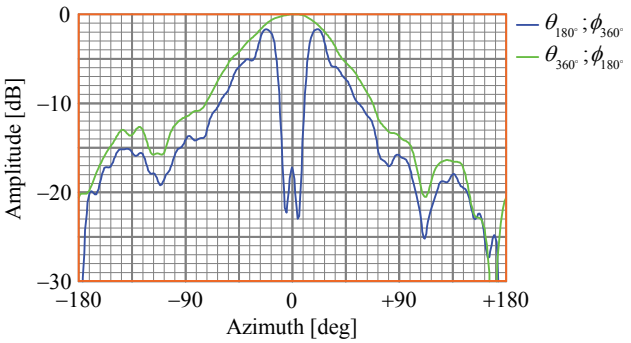

Figure 17: Can Antenna ($\phi = 0$ deg)

Electrical alignment is used to correct for any mechanical deviations. Two cuts along the same plane are measured, with the polarisation of the AUT rotated by 180° between cuts, with any deviation between the cuts attributed to a mechanical misalignment. A discrepancy in the amplitude between the two cuts indicates the offset from the axis, as depicted in Figure 18, while a discrepancy in the phase indicates the offset from the mounting interface.

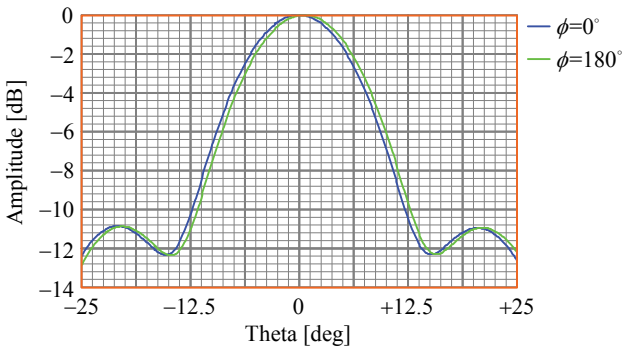

Figure 18: Alignment Check

5.3 *Determining Chamber Reflection Levels*

The effect of exposed reflective surfaces in the chamber has been investigated using SNF measurements of a standard gain horn with the WR137 probe, as depicted in Figure 19. The probe is shielded from reflections off the Y Tower by its collar, as indicated by the marginal effect on the pattern when the gap between the absorber panels is narrowed. Similarly, the probe is shielded from reflections

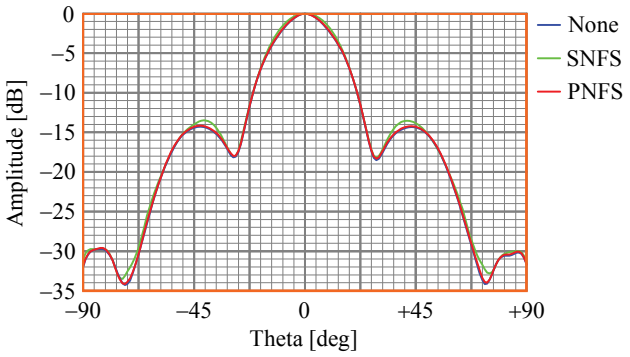

Figure 19: Reflection Check ($\phi = 0$ deg)

off the L Bracket by the AUT's collar, as indicated by the noticeable effect on the pattern when this collar is added.

The absorber pyramids that the chamber is covered with are specified down to 1 GHz; however it is desirable to extend use of the chamber down to at least 0.75 GHz. Therefore, the method outlined in [8, §8.10] has been used to quantify the level of reflection from the chamber at low frequencies. The underlining principal is that if the distance between the AUT and the source of reflection is changed by $\lambda/4$, the comparison between the two measurements can be used to separate the desired signal from the reflected signal.

As an example, measurements have been taken to determine the chamber reflection at 0.75 GHz, which is below the lower limit specified for the absorber pyramids, as depicted in Figure 20. The probe and the AUT are separated by a fixed distance for the first measurement, with both translated by $\lambda/4$ for the second. The effect of reflections off the probe is equivalent in both measurements, as the separation between the AUT and probe remains constant. The result indicates a chamber reflection level of below -30 dB.

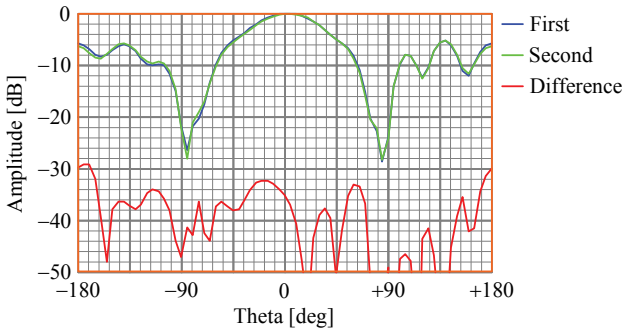

Figure 20: Chamber Reflection

A feature of our indoor antenna range is the ability to take redundant SNF measurements. The AUT can be rotated 360° around both the θ axis and the ϕ axis, resulting in the radiated fields over the full sphere being sampled twice, but with different configurations of the AUT with respect to the chamber. For instance, a full NF measurement can be performed with the AUT rotated from 0° to +180° around the θ axis, which directs the AUT towards one side of the chamber, and a full redundant NF measurement can be performed with the AUT rotated from 0° to −180° around the θ axis, which directs the AUT towards the other side of the chamber, as depicted in Figure 21. For both measurements, the AUT is rotated 360° around the ϕ axis.

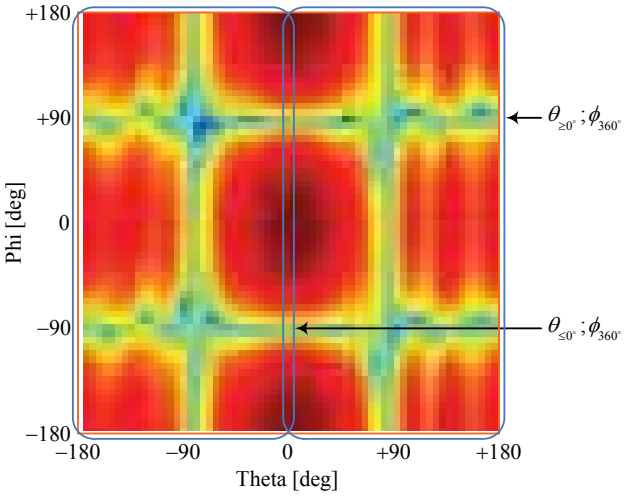

Figure 21: Redundant Near-Field Measurement

Theoretically, these two SNF measurements should transform to equivalent FF patterns. However, the poor absorptive properties of the absorber material used in our chamber at lower frequencies, and especially below the specified 1 GHz limit, result in radiated fields being reflected off the walls of chamber back towards the probe. The offset position of the SNF scanner to make room for the walkway results in a disparity in the signal path on opposite sides of the AUT, which is more pronounced at lower frequencies. The combination of these two phenomena result in a disparity in the radiated fields detected by the probe when the AUT is directed to the opposite sides of the chamber at 0.75 GHz, as depicted in Figure 21.

This disparity between the NF measurements results in a variance between the computed FF patterns. This variance is more pronounced at lower frequencies than at high frequencies, as depicted in Figure 22. For example, the RMS value between the two principal Azimuth cuts is -25.3 dB at 0.75 GHz, while at 3 GHz it is -32.3 dB. To quantify the disparity between the two sets of redundant SNF measurements, the RMS difference between the two sets of computed FF patterns is calculated over the whole sphere for a range of frequencies, as depicted in Figure 23. As expected, this disparity is larger at lower frequencies, especially below the specified 1 GHz limit, and it is not improved by replacing the walkway with pyramids.

Using these calculated RMS values, the measurement uncertainty in the computed FF patterns at 0.75 GHz is depicted in Figure 24. Depending on the measurement configuration, the actual FF pattern of the AUT would be

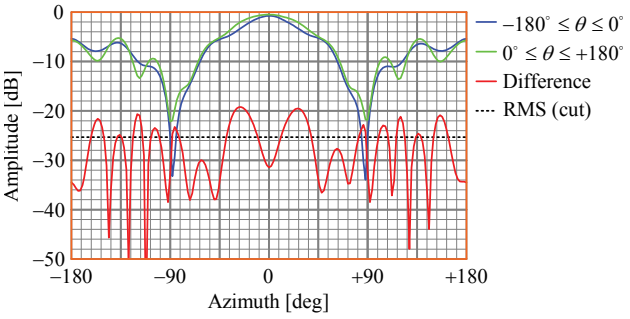

(a) 0.75 GHz

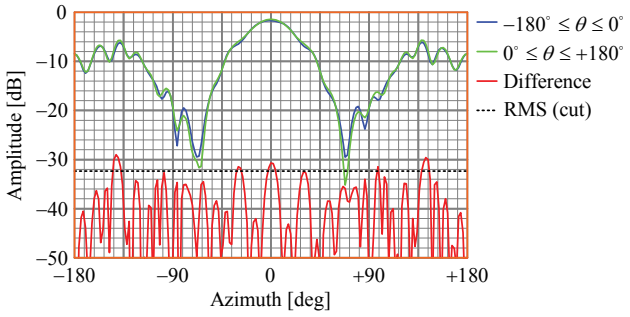

(b) 3.0 GHz

Figure 22: Redundant Spherical Measurements

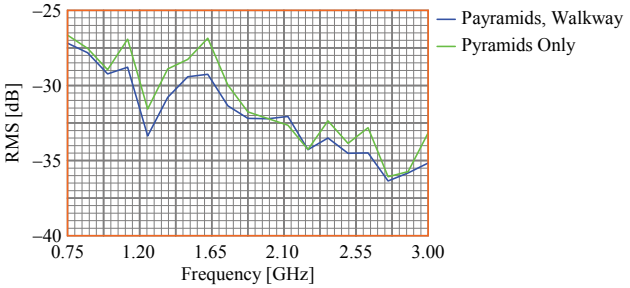

Figure 23: RMS Disparity between Computed Far-Field Patterns

within the RMS envelop around the computed FF pattern. (The specific AUT in this case is a commercial biconal antenna, with operating band 500 MHz — 3 GHz). Such a plot could be used to determine the certainty with which the measured AUT meets the design requirements.

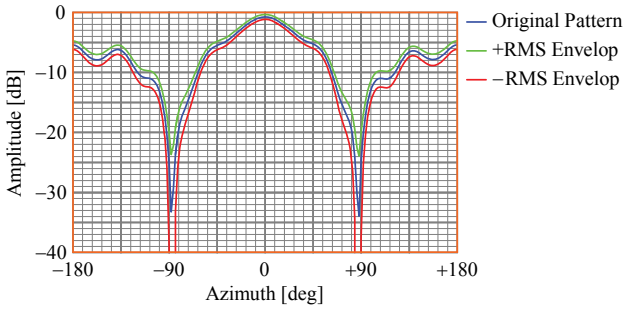

Figure 24: Far-Field Cut with RMS Envelop

5.4 Measured Results for a Patch Antenna

To demonstrate the functionality of the antenna range, the FF patterns of a circular polarised patch antenna were determined. This antenna operates over the 2.4 GHz to 2.5 GHz frequency range and has dimensions of 32 cm (L) × 8 cm (W). As the FF starts at 1.75 m, the FF patterns can be determined by transforming NF measurements into FF data or by taking FF measurements. Both options were chosen, to compare the results of these two types.

For the measurements, the horn probe was attached to the PNF scanner, and the patch antenna was attached to the SNF scanner. The only change to the measurement setup between measurements, was to shift the SNF scanner along the Z Track, moving the probe from inside the radiating NF to the FF. To validate the comparison, the measurements were performed to generate equivalent FF data sets, that of a θ span of 261° and a ϕ span of 360°, at intervals of 3°.

For the FF measurement, the AUT to probe separation was 4.9 m, with a scan area of 261° (θ) × 360° (ϕ) sampled at 3° intervals. For the NF measurement, the probe scan radius was 1 m and the minimal radius sphere was 0.16 m, with a scan area of 171° (θ) × 360° (ϕ) sampled at 9° intervals. While the measurement times are equivalent, the data processing software can zero pad the NF data to improve the resolution of the projected FF data.

Both measurement types provide accurate patterns of the antenna, with the principal cuts at 2.45 GHz for the two measurement sets depicted in Figure 25. The difference between the two results is minimal, less than 2 dB on the flanks of the main lobe and less than 4 dB for the side lobes. This discrepancy is as a result of the difference in the environment between the two measurement sets; in changing the separation, the signal path was changed.

6. FUTURE WORK

The necessity to improve the absorber coverage in the anechoic chamber is under investigation. The focus is on components that are visible to the probe, as it is the probe's response to the signal transmitted by the AUT that is measured. The SNF scanner will receive attention in the form of an absorber coverage for its base and the PNF scanner will receive attention in the form of absorber coverage for the X Track for SNF measurements.

Work is in progress to expand the frequency range of the anechoic chamber. To bridge the gap between the specified ranges of the probes, a standard gain horn will be measured using the probes, to determine whether the probes can be used outside of their specified ranges. To extend the frequency range beyond 18 GHz, an additional probe would be required, along with the RF cabling and connectors required to deliver the RF signal to the VNA.

The power amplifier, housed on the Y Tower, amplifies the signal levels that are detected by the probe before they are delivered to the VNA. However, the stability of this

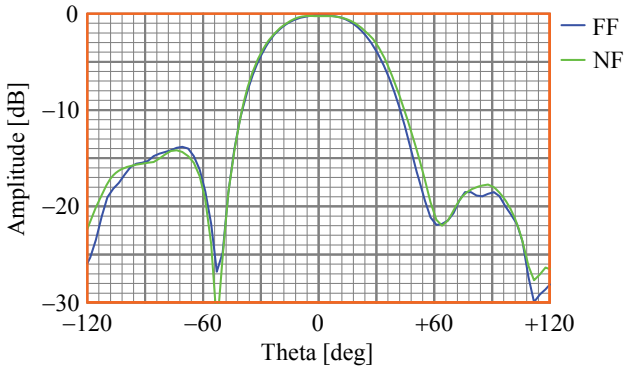

(a) $\phi = 0$ deg

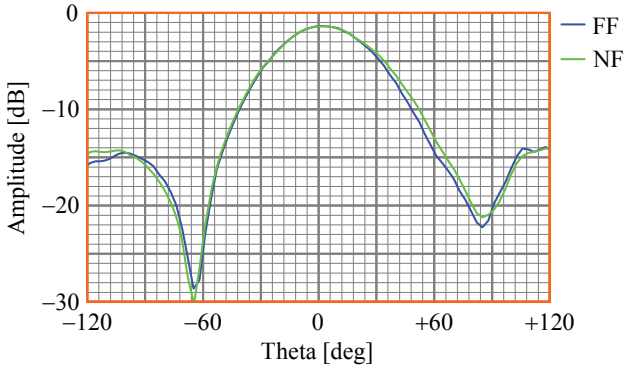

(b) $\phi = 90$ deg

Figure 25: Principal Polarisation Cuts

amplifier is neither monitored nor controlled at present. An improved system would be to position an appropriate amplifier at the input to the VNA, making it a part of the measurement setup, with the performance of this amplifier controlled and monitored by the data processing software.

The motors are run in open-loop mode, with no feedback to control these motors' motions — nor is there an independent monitoring system for this. An improved system would be to install laser trackers to monitor the translation of the x stage and y stage. These trackers would be housed behind the absorber panels, to minimise any influence on the measurements. The data processing software would use this data to adjust the sample positions.

Although there are at present no plans to do this, it is worth stating that most, if not all, of the hardware and software required to perform CNF measurements are in place. The θ stage would provide the ϕ rotation and the y stage would provide the z translation, thereby requiring both the probe and the AUT to move throughout the measurement process. Should the specific requirements arise for a CNF scanner, it could be implemented at a very reasonable cost.

The mounting interfaces of the scanners are compatible with the probes, permitting the probes to be mounted on either scanner. However, the mounting interfaces of the scanners are not compatible with all potential AUTs. Over time, as different AUTs are measured, additional mounting brackets will be manufactured. This increase in the variety of brackets is expected to assist future measurements.

The cabling interface between the new components in the control room is different to that of the previous components. This requires a redesign of the cabling from the VNA to the interface with the anechoic chamber. There is a stability problem with the cabling at the rear of the PNF scanner, with corrective measures being pursued in the form of a pulley system and more phase-robust cabling.

7. CONCLUSION

The substantial upgrade that Stellenbosch University's indoor antenna range underwent in October 2014 has been described, as well as the initial commissioning tests. The result is the availability of FF, PNF and SNF measurements over a wide frequency range, potentially spanning from 1 GHz up to 26.5 GHz. The lower limit is set by absorber performance and the upper limit is set by the VNA. For a particular antenna, while the frequency range and directivity could suggest a particular measurement type, the weight, dimension and rigidity of the AUT could preclude, or at least depreciate, the use of certain measurement types.

This upgrade has greatly improved the ability to control and interact with the antenna range. The calibration process provides sanity checks to ensure proper configuration. The measurement process gives regular feedback, displaying intermediate measurements. The powerful processing system performs probe corrections and NF to FF transformations, as well as exporting data for analysis. The new NF capabilities have facilitated the evaluation of the chamber, such as using multiple and redundant measurements to evaluate the level of chamber reflections.

Whilst the chamber is primarily intended for Stellenbosch University staff and students, it is available to outside organisations*. The original antenna range provided almost three decades of service to Stellenbosch University's research and teaching programs in RF and microwave engineering. Given the longevity of its predecessor, it is hoped that the new facility will provide service well into the 21st century!

ACKNOWLEDGEMENTS

Funding for this major upgrade was provided by the National Research Foundation's National Equipment Program; Square Kilometre Array South Africa; the Department of Science and Technology's Research Chair Initiative; and Stellenbosch University's Strategic Fund and Engineering Faculty. All of these funding sources are acknowledged for covering the cost of approximately US$ 400 000 at the time of procurement.

*Those interested in using this facility are invited to contact the laboratory manager, Anneke Bester (annekeb@sun.ac.za) at the time of writing, who can provide mechanical drawings of the scanner interfaces to assist in the manufacture of compatible interfaces for their own devices. Raw and processed NF and FF data can be exported using a scripting tool.

This antenna range functions under the auspices of Stellenbosch University's Central Analytical Facilities Affiliated Instruments program, whose support during the procurement process is acknowledged.

The physical installation was performed by D. J. J. van Rensburg and P. N. Betjes (both of NSI), W. Croukamp (of Stellenbosch University), and the authors. Equipment, such as the SNF base as well as the brackets for the AUTs and the chamber reflection measurements, was designed and manufactured by W. Croukamp. The installation team is gratefully acknowledged, as is NSI's Project Manager, C. Smith. The photographs were taken by A. Jordaan (of Stellenbosch Centre for Photographic Services).

REFERENCES

[1] C. F. du Toit, J. Solms, K. D. Palmer, and J. H. Cloete, "Recent Progress on Cylindrical Near Field Antenna Measurements at Stellenbosch University," in *Proceedings of Joint Symposium on AP/MTT*, Pretoria, August 1988.

[2] D. E. Baker, "Evaluation and Modification of the NIAST Microwave Anechoic Chamber," in *Proceedings of Joint Symposium on AP/MTT*, Pretoria, August 1986.

[3] D. J. J. van Rensburg and C. W. I. Pistorius, "Compact Antenna Test Range at the University of Pretoria," in *Proceedings of AFRICON Conference*, Ezulwini Valley, September 1992.

[4] D. E. Baker, "User Manual for General Antenna Related Measurements at the National Antenna Test Range at Paardefontein," Gerotek Test Facilities, Paardefontein, Tech. Rep. 04/2010, August 2010.

[5] J. L. Jonas, "MeerKAT – South African Array With Composite Dishes and Wide Band Single Pixel Feeds," *Proceedings of the IEEE*, vol. 97, no. 8, pp. 1522–1530, August 2009.

[6] J. E. Hansen, *Spherical Near Field Antenna Measurements*. London: IET, 1988.

[7] D. Slater, *Near Field Antenna Measurements*. Boston, MA: Artech House, 1991.

[8] C. Parini, S. Gregson, J. McCormick, and D. J. J. van Rensburg, *Theory and Practice of Modern Antenna Range Measurements*. London: IET, 2015.

[9] D. E. Baker and R. Booysen, "High Performance Tapered Anechoic Chamber for 0.5 to 40 GHz," in *Abstracts of the SA IEEE Joint AP/MTT/EMC Conference*, Stellenbosch, April 2011.

[10] Nearfield System, Inc. Torrance. [Online]. Available: http://nearfield.com

[11] "Keysight 2-Port and 4-Port PNA-X Network Analyzer: Data Sheet and Technical Specifications," Keysight Technologies, Santa Rosa, Tech. Rep. N5242-90007, November 2014.

[12] C. A. Balanis, *Antenna Theory: Analysis and Design*, 3rd ed. Hoboken, NJ: Wiley, 2005.

[13] A. D. Yaghjian, "Approximate Formulas for the Far Field and Gain of Open Ended Rectangular Waveguide," *IEEE Transactions on Antennas and Propagation*, vol. 32, no. 4, pp. 378–384, April 1984.

[14] P. Pelland and A. Newell, "Combining Pattern, Polarisation and Channel Balance Correction Routines to Improve the Performance of Broad Band, Dual Polarised Probes," in *Proceedings of AMTA Meeting and Symposium*, Tucson, October 2014.